Box inverse models, altimetry and the geoid: Problems with the omission error

Martin Losch,[1,4] Bernadette M. Sloyan,[2,5] Jens Schröter,[1] and Nico Sneeuw[3,6]

[1] When one combines satellite altimetry and a geoid model to improve estimates of the ocean general circulation from hydrographic data with a box inverse model, there arises a problem of different resolution and representation of the data types involved. Here we show how this problem can lead to an artificial leakage of the error estimates of short-scale (high degree) spherical harmonic functions into long wavelength (low wave number) Fourier functions. A similar paradox effect can be seen in an idealized box inverse model constrained by additional sea-surface topography data of low, medium, and high resolution: When more information is added in the form of additional smaller scales, the error of a transport estimate eventually increases. Consequently, including the large geoid omission errors associated with smaller scales in a box inverse model of the Southern Ocean increases the posterior errors of transport estimates over those of a model that does not include the geoid omission error. We do not claim that including or excluding the geoid omission error is correct. Instead, we juxtapose two different ways of estimating the geoid errors to demonstrate the effect that the omission error might have on the long, supposedly well-known, scales. How (or if) to properly account for the geoid omission error must be the topic of further research. A proper treatment of the geoid model errors is demanded when one evaluates the errors of absolute sea-surface topography data. *INDEX TERMS:* 3337 Meteorology and Atmospheric Dynamics: Numerical modeling and data assimilation; 1243 Geodesy and Gravity: Space geodetic surveys; 1227 Geodesy and Gravity: Planetary geodesy and gravity (5420, 5714, 6019); 4263 Oceanography: General: Ocean prediction; 4532 Oceanography: Physical: General circulation; *KEYWORDS:* Ocean general circulation, inverse modeling, satellite altimetry, geoid modeling, omission error

1. Introduction

[2] Estimating the absolute ocean circulation is one of the major tasks of physical oceanography. Some of the efforts that are currently undertaken include various types of numerical ocean models in conjunction with data assimilation techniques and inverse methods [*Wunsch*, 1978; *Fu*, 1986; *Roemmich and McCallister*, 1989; *Rintoul*, 1991; *Macdonald*, 1998; *Sloyan and Rintoul*, 2001b; *Malanotte-Rizzoli*, 1996; *Fukumori*, 1995; *Stammer et al.*, 1997; *Bell et al.*, 2000; *Wenzel et al.*, 2001]. The success of these models is critically dependent on the amount and the type of observational data. From the available data, sea-surface topography measurements from satellite altimetry have the potential to provide the best coverage and resolution for all ocean regions. Also, they reflect the three-dimensional flow best when compared with other surface data [*Wunsch and Stammer*, 1998].

[3] TOPEX/Poseidon and ERS2 satellite altimetric missions presently provide extraordinarily accurate and precise data. However, the use of this information has largely been limited to studies of time-dependent phenomena in the ocean [e.g., tides: *Egbert*, 1997; *Le Provost et al.*, 1998], which only require information on the sea-surface height anomaly. To use satellite altimetry data in the steady state ocean problem or for estimating the absolute circulation, one has to reference the altimetric height to the marine geoid to determine the dynamic sea-surface topography. Uncertainties associated with the marine geoid exceed those of the altimetry by an order of magnitude, rendering the estimated dynamic sea-surface topography very noisy.

[4] At present there are numerous estimates of the marine geoid to which the satellite altimetry can be referenced. *Ganachaud et al.* [1997], using a global "box" inverse model, investigated factors that limit the use of satellite altimetry in studies of the mean ocean circulation. They concluded that our present knowledge of

---
[1]Alfred-Wegener-Institut für Polar- und Meeresforschung, Bremerhaven, Germany.
[2]NOAA/Pacific Marine Environmental Laboratory, Seattle, Washington, USA.
[3]Institut für Astronomische und Physikalische Geodäsie, Technische Universität, München, Germany.
[4]Now at Department of Earth, Atmospheric, and Planetary Sciences, Massachusetts Institute of Technology, Cambridge, Massachussetts, USA.
[5]Now at Department of Physical Oceanography, Woods Hole Oceanographic Institution, Woods Hole, Massachusetts, USA.
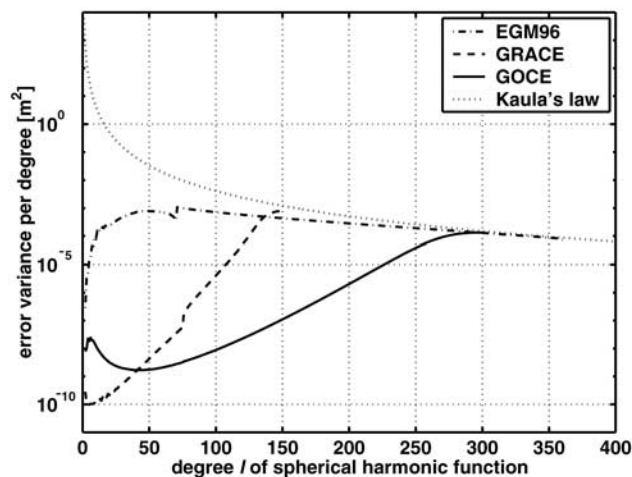[6]Now at Department of Geomatics Engineering, University of Calgary, Alberta, Canada.

Figure 1. Spherical harmonic error variance per degree of the geoid models EGM96, GRACE, and GOCE, in comparison with Kaula's law (model signal variance) [after *Balmino et al.*, 1998].

the marine geoid (they used the JGM-3 geoid model) is inadequate to significantly improve estimates of the mean circulation. New dedicated satellite gravity missions will determine very accurate geoid models: Gravity Recovery and Climate Experiment (GRACE) [*Tapley*, 1997] and Gravity field and steady-state Ocean Circulation Explorer (GOCE) [*Battrick*, 1999]. As a result of these respective missions, a marine geoid will become available that will be orders of magnitude more accurate than the "state-of-the-art" EGM96 model [Earth Gravitational Model 1996, *Lemoine et al.*, 1997] (Figure 1). The highly improved geoid models will lead to a wide range of new applications of sea-surface height data to oceanographic problems.

[5] Given that we will have an accurate marine geoid in the near future, it is appropriate to again address some of the issues raised by previous studies [e.g., *Wunsch and Gaposchkin*, 1980; *Ganachaud et al.*, 1997]. In these studies the authors found that an inaccurate marine geoid model inhibits satellite altimetry data from improving the estimate of the ocean circulation. *LeGrand* [2001] and *Schröter et al.* [2002] investigated the influence of additional sea-surface topography information with higher resolution on the determination of the steady state ocean circulation. These authors found that with altimeter data and an accurate geoid model derived from the gravity data of GRACE and GOCE, the errors of estimated integrated volume and heat transports can be reduced by up to 50%.

[6] In this paper we will discuss the more general problem of combining satellite altimetry, the marine geoid, and an ocean model into an estimate of the ocean circulation. The information from these three sources all have different resolutions and representations, thus the scales that the three signals and their errors describe and omit are different. In order to compare satellite altimetry and the marine geoid with the sea-surface topography estimated by an ocean model in the context of inverse methods, it will be necessary to match their scales by applying a suitable filter.

[7] Geoid models are generally given as an expansion into spherical harmonic functions; therefore a filter with a boxcar or Dirichlet kernel appears simplest and most effective. Compared to the amplitudes of the geoid undulations of the order of 100 m relative to a reference ellipsoid, the errors due to truncation of a geoid model at a certain degree are small. Modeled geoid errors, however, are small for low degrees (large scales) and orders of magnitude larger on high degrees (small scales). Therefore the truncation at a low degree neglects large error contributions which, however, is justified because the neglected error is orthogonal to the geoid model.

[8] In an oceanographic context, it is more natural to think in terms of wavelengths than in spherical harmonic functions. On oceanography domains, which do not cover the entire globe, the formerly neglected geoid error no longer is orthogonal to the resolved signal. Because of its relative magnitude, this omitted error can have significant contributions to the resolved long wavelengths. Therefore the spherical harmonic boxcar filter is not optimal for domains that do not cover the entire globe, but finding a filter that performs adequately on all three sources of information appears to be difficult. Consequently, the use of sea-surface height data in inverse models or data assimilation is not straightforward because both the description of the signals and the errors have a substantial influence on the solution obtained from these methods.

[9] Unfortunately, accurate geoid data are not currently available. This makes it difficult to study the impact of suboptimal filtering on estimates of the circulation itself. Instead, the influence of the filtering can be assessed using the predicted error covariance of the new gravity missions, GRACE and GOCE. Again, these errors are very small on long scales, so that the possible impact of large errors on short scales becomes apparent. This paper will demonstrate the impact of two different filtering methods of sea-surface topography information in a box inverse model of the Southern Ocean.

[10] In section 2 we briefly discuss the components of sea-surface topography data and model errors. In this context we need the term "omission" error to describe the unresolved part of the signal. The problem stemming from different resolutions and representations is also raised. Section 3 illustrates this problem with the help of a simplified version of a box inverse model in an artificial scenario. Section 4 shows two extremes of the impact of sea-surface topography data on the estimates of a realistic box inverse model when one does or does not take into account the omission error of the geoid model. The sea-surface topography data is generated by the model itself to avoid possible problems stemming from inconsistencies of hydrography, model, and satellite data. We use two different filtering methods to combine data and model. We do not claim that either of these methods is correct. The results of the two filtering methods, which differ greatly, are juxtaposed to demonstrate the effect that the geoid omission error might have on the long, supposedly well-known, scales. The reader should keep in mind that it is not our intention to find the "correct" filter method. (Such a filter could be a compromise between the two extremes described in this paper.) How (or if) to properly account for the geoid omission error must be the

topic of further research. The conclusion and summary are given in section 5.

2. Sea-Surface Topography Data

[11] We confine the a priori error discussion in this section to errors of the sea-surface topography data, as this is the topic of this paper. The errors of other types of data or other model variables depend on the specific model and data type and are not considered here.

[12] For the discussion we borrow a terminology from geodesy. There the term ''commission'' error describes the part of the Earth gravity field that is resolved by a specific geoid model. Likewise the ''omission'' error refers to the unresolved, unmodeled part of the gravity field. We extend the use of these terms to models of the ocean circulation. The geodetic commission and omission errors are defined in a purely spectral way since the geoid models are usually formulated in spherical harmonic functions. By contrast, models of the ocean circulation are generally not formulated in a spectral representation, let alone in spherical harmonics. We will use the term ''omission error of the oceanographic model'' to describe the errors introduced by approximating the differential equations of the model on a computational grid with a finite resolution. In the same manner a gridded data set of sea-surface height has an omission error due to the finite resolution of the grid. In general, the omission error is the signal that has not been modeled.

2.1. Data and Model Errors

[13] The sea-surface topography of an oceanographic model can be calculated from the general principle of geostrophy [Pedlosky, 1987]. Owing to the simplifications of the momentum equations that lead to geostrophy, the sea-surface height contains errors that could be estimated in principle. For practical reasons we neglect these errors here. We only keep in mind that there is an omission error of the oceanographic model because of the finite resolution of the model grid. The maximum resolution of the model grid can vary in space with the local grid step size.

[14] The absolute sea-surface topography ζ^* determined from satellite measurements is the difference between the sea-surface height h relative to a reference ellipsoid and the geoid height N over the same reference ellipsoid: $\zeta^* = h - N$. If h and N are uncorrelated, the error covariance of ζ^* is the sum of the error covariances of h and N:

$$C_\zeta = C_N + C_h. \qquad (1)$$

This equation describes the valid assumption that N and h stem from different sources of data, which are independent (altimetry and geoid model). However, equation (1) is only valid for the commission errors of N and h. Because the omission errors technically consist of the unmodeled signals, which do not have to be independent, one cannot assume that the errors due to omitting these signals obey equation (1).

[15] The sea-surface height h relative to a reference ellipsoid is measured by satellite altimetry. The commission error of h consists of actual measurement errors and, if h represents an estimate of the mean, deviations from the mean. The omission error due to interpolation between satellite ground tracks should also be accounted for as in, for example, the mean sea-surface CLS_SHOM98.2 by *Hernandez and Schaeffer* [2000]. There the spatial distribution of the estimated errors exhibits a ''trackiness'' with small values along the ground tracks of the TOPEX/Poseidon satellite and larger values in between satellite tracks. Along the ground tracks the omission error can probably be neglected since the along track resolution is very high. However, for a gridded data set of h, the longest scale of the omission error is determined by the grid step size.

[16] The geoid height N is generally calculated from a geoid height model. Such a model is defined on the entire globe and therefore naturally represented in terms of fully normalized spherical harmonic functions $Y_{lm}(\theta, \lambda)$:

$$N(\theta, \lambda) = R \sum_{l=2}^{\infty} \sum_{m=-l}^{l} y_{lm} Y_{lm}(\theta, \lambda), \qquad (2)$$

where l is the degree of the spherical harmonic, m is the order, and y_{lm} is the corresponding spherical harmonic coefficient. The mean radius of the Earth is R, the colatitude is θ, and longitude is λ. The spherical harmonic functions are defined as

$$Y_{lm}(\theta, \lambda) = \sqrt{\frac{(2l+1)}{4\pi} \frac{(l-m)!}{(l+m)!}} \, P_{lm}(\cos \theta) e^{im\lambda},$$

with the associated Legendre functions P_{lm}. The geoid height error covariance between two points (θ, λ) and (θ', λ') is

$$C_N(\theta, \lambda, \theta', \lambda') =$$
$$R^2 \sum_{l=0}^{L} \sum_{m=-l}^{l} \sum_{l'=0}^{L} \sum_{m'=-l'}^{l'} Y_{lm}(\theta, \lambda) \langle \delta_{y_{lm}}, \delta_{y_{l'm'}} \rangle Y_{l'm'}(\theta', \lambda'), \qquad (3)$$

with the coefficient error covariance $\langle \delta y_{lm}, \delta y_{l'm'} \rangle$. In practice, series (2) is truncated at a maximum degree L. This is justified as y_{lm} drops with approximately $1/l^2$ according to Kaula's rule [*Kaula*, 1966], so that the neglected y_{lm} are orders of magnitude smaller than the y_{lm} for small l (Figure 2).

[17] However, the geoid commission errors δy_{lm} do not follow this asymptotic behavior. Instead the error is smallest for small l and increases rapidly with increasing l. The maximum degree L is conventionally chosen as the point where the modeled signal-to-noise ratio, that is, y_{lm} versus δy_{lm}, becomes one. This point is usually referred to as the resolution of the gravity field solution. By a rule of thumb, this resolution is half-wavelength, that is $\pi R/L$. Kaula's signal variance model assumes the role of an error variance for $l > L$, since no better information on the y_{lm} is available. This part of the spectrum constitutes the omission error of the geoid model.

[18] In general the resolutions of the oceanographic model, the sea-surface height h relative to the reference ellipsoid, and the geoid height N are different. Also, the resolution of the oceanographic model can vary in space, for example, if the grid is determined by stations along a hydrographic section, or if it is any nonuniform grid. The different resolutions of model and data values determine the
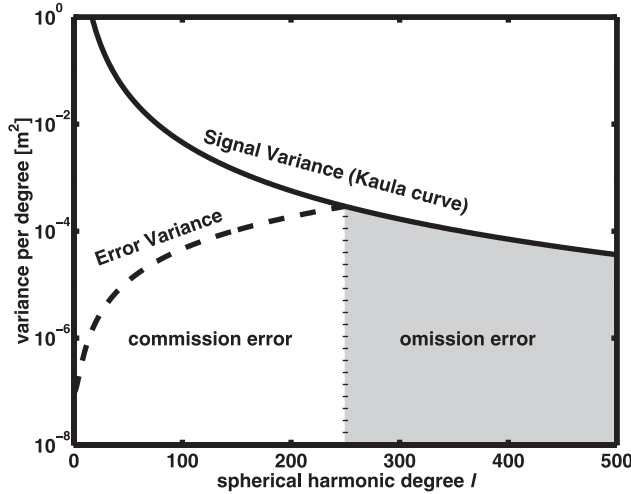
Figure 2. Schematic plot of signal variance per degree using Kaula's law and a synthetical error spectrum.

respective omission errors. Therefore when comparing model sea-surface topography with $h - N$, it is necessary to find a common resolution of model and data values so that the signal and the commission errors of the three components describe the same wavelengths. This common resolution is determined by the smallest resolution available, which is generally the geoid model resolution.

2.2. Concept of Wavelength

[19] On a torus, a rectangular plane, or a straight line the concept of wavelength is clear. Each wavelength can be associated with a harmonic function of these domains, namely the trigonometric functions sine and cosine. The shortest wavelength that can just be represented on a uniform grid on these domains is the Nyquist wavelength.

[20] The definition of wavelength is less clear when we want to attribute wavelengths to the spherical harmonic degree. As a rule of thumb one attaches $\pi R/l$ as half-wavelength or spatial scale to any degree l. This is due to the fact that an associated Legendre function of degree l and order $m = 0$ has l zero crossings on the interval $\theta \in [0; \pi]$, although not equi-angularly spaced. Attaching a wavelength to a degree l is imprecise for two reasons. First, for any degree l, we have a whole range of orders (also known as azimuthal wave number) $m = 0, \ldots, l$ appearing as $\cos m\lambda$ and $\sin m\lambda$ in the spherical harmonic functions. In the Fourier analogy, one would try to obtain a one-dimensional (1-D) Fourier spectrum by averaging a two-dimensional (2-D) Fourier spectrum in one direction. Second, any associated Legendre function P_{lm} can be represented as a sum of trigonometric functions:

$$P_{lm}(\cos \theta) = \sum_{k=0}^{l} a_{lmk} \begin{cases} \cos k\theta & \text{if } m \text{ even} \\ \sin k\theta & \text{if } m \text{ odd} \end{cases}, \quad (4)$$

with vanishing a_{lmk} for odd $l - k$ [*Sneeuw and Bun*, 1996]. Thus any associated Legendre function of degree l contains contributions from all wave numbers $k \leq l$. This will become even clearer from the simpler case discussed in the following paragraphs.

[21] In this paper we consider only geoid models with homogeneous, isotropic errors. Away from polar areas, that is a valid assumption for the satellite missions under considerations. By making this assumption and by applying the addition theorem of spherical harmonics, the covariance function (3) is simplified to a series of Legendre polynomials:

$$C(\psi) = \sum_{l=0}^{L} p_l P_l(\cos \psi), \quad (5)$$

where ψ is the spherical distance between two points (θ, λ) and (θ', λ') on the sphere. The coefficients p_l are the geoid degree variances, $R^2 \sum_{m=-l}^{l} \langle \delta y_{lm}, \delta y_{lm} \rangle$. This representation is invariant under rotations on and over the sphere.

[22] For a Legendre polynomial P_l, which is an associated Legendre function with azimuthal wave number $m = 0$, equation (4) reduces to a series of cosines with maximum wave number $k_{\max} = l$:

$$P_l(\cos\psi) = \sum_{k=0}^{l} a_{lk} \cos k\psi, \quad (6)$$

again with vanishing a_{lk} for odd $l - k$. The absolute values of a_{lk} decrease for increasing $(l - k)$. Thus the main contribution to a Legendre polynomial $P_l(\cos\psi)$ would be $a_{ll} \cos l\psi$. Consequently, a Legendre polynomial of a certain degree strongly resembles a cosine with wave number equal to that degree, which is the rationale for the aforementioned rule of thumb.

[23] Inserting equation (6) in the above covariance function equation (5), we have:

$$\begin{aligned} C(\psi) &= \sum_{l=0}^{L} p_l \sum_{k=0}^{l} a_{lk} \cos k\psi \\ &= \sum_{k=0}^{L} \sum_{l=k}^{L} p_l a_{lk} \cos k\psi \\ &= \sum_{l=k}^{L} c_k \cos k\psi, \end{aligned} \quad (7)$$

with the coefficients

$$c_k = \sum_{l=k}^{L} p_l a_{lk}. \quad (8)$$

This latter formula, with reordered wave numbers and degrees, shows that a given power spectral coefficient c_k (in Fourier sense), pertaining to a certain wave number k, contains contributions of degrees $l = k$ up to L. Thus changing the maximum degree L automatically changes the power of the entire Fourier spectrum.

[24] Figure 3 illustrates this behavior for the expected isotropic and homogeneous GOCE error covariance function. More important, it is seen that the coefficients a_{lk} in equation (8) are multiplied by the degree variances p_l in order to provide the coefficients c_k. Thus the decreasing behavior of the a_{lk} does not automatically carry over to the Fourier coefficients.

[25] This is exactly what will happen in the case of geoid error covariance functions from gravity field missions as demonstrated by Figure 2. The spherical harmonic geoid error spectrum may vary over several orders of magnitude
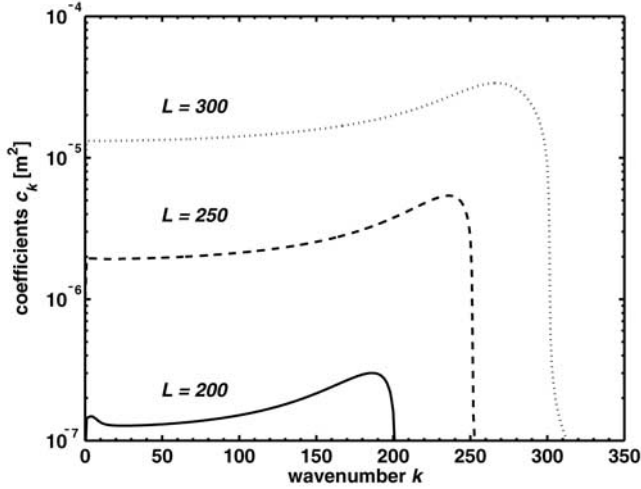
Figure 3. Fourier spectra of GOCE geoid error covariances with different maximum degree L.

with the smallest degree variances at the low degrees. This is already unfavorable for the calculation of c_k. The situation becomes worse when the omission error is taken into account. Beyond the maximum degree of resolution L, the signal degree variance takes the role of an error degree variance. Although the level of the omission error decreases slowly for increasing degree, it remains at a considerably high level for a large range of degrees. This whole range will project onto the low wavenumber Fourier spectrum by virtue of equation (8).

[26] What we have described so far is hardly more than what usually occurs when one makes a change of basis from one set of orthogonal functions to another set. However, this change of basis can become a problem in oceanographic applications because no ocean model domain covers the entire sphere. Consequently, spherical harmonic functions are not a convenient basis for describing the marine geoid, since they are not orthogonal on a fraction of a sphere. Neither are the trigonometric functions orthogonal on such a domain. They have been used only to illustrate the problem. However, this problem arises with any change of basis, its severity depending on the shape of the model's domain, that is, by how much the domain differs from the full sphere.

[27] Taking the problem to the extreme, one could include the complete geoid omission error into the calculation of the error covariances of the signal to degree and order L. We assume an isotropic and homogeneous omission error covariance function and estimate its coefficients using Kaula's rule [Kaula, 1966]. We arrive at the following formulation for the geoid height error covariances:

$$C_N(\theta, \lambda, \theta', \lambda') = C_N^{(L)}(\theta, \lambda, \theta', \lambda') + R^2 \sum_{l=L+1}^{\infty} \kappa_l P_l(\cos \psi). \quad (9)$$

The commission error $C_N^{(L)}(\theta, \lambda, \theta', \lambda')$ is calculated from the series (3) and truncated at a certain maximum degree L.

$$\kappa_l = \frac{10^{-10}(2l+1)}{2l^4} \approx 10^{-10} l^{-3} \quad (10)$$

is the signal variance according to Kaula's rule of thumb. The second term in equation (9) represents the omission error. In practice, it is impossible to extend the sum in equation (9) to infinity. Therefore, given the finite resolution of the inverse ocean model used in this paper, which is at best $(1/3)°$ spherical distance, we decided to stop the summation at $l = 1000$, which corresponds approximately to a wavelength of that size. Also at this degree the cumulative sum of the Kaula signal variance is no longer increasing rapidly. It is well known that Kaula's rule does not adequately describe the anomaly degree variances for degrees higher than 1000. For this range other rules may be used [Rapp, 1972]. These are in principle similar; that is, they describe the spherical harmonic coefficient variance as a function of l but, at the same time, ensure that the sum in equation (9) remains finite. However, for the purpose of our study we used the more familiar Kaula rule, which is almost as good and describes variances below $L = 1000$ accurately [Rapp, 1972].

[28] A geoid error covariance function C_N calculated by equation (9) contains contributions at wavelengths down to $2\pi R/1000$. We remove these short scales by applying a Butterworth low-pass filter to the covariance function C_N with a cut-off wavelength of $2\pi R/L$ [e.g., Kulhánek, 1976]. The resulting $\overline{C_N}$ is an estimate of the geoid height error covariance only for the long wavelengths, where now long means longer than $\lambda = 2\pi R/L$.

[29] Figure 4 illustrates the effect of our procedure. Shown are the Fourier power spectra of the GOCE covariance functions, where the Legendre series (3) has been truncated at degree $L = 200$ (dotted line) and $L = 1000$ (dashed line). As before, the power of the long wavelengths increases with increasing L. Here the increase is over 3 orders of magnitude. Also shown is the power spectrum of the covariance function to degree 1000 after application of the Butterworth low-pass filter with a cut-off wavelength $2\pi R/k$, $k = 200$ (solid line). For this covariance function the power of the long wavelengths is independent of k, where k
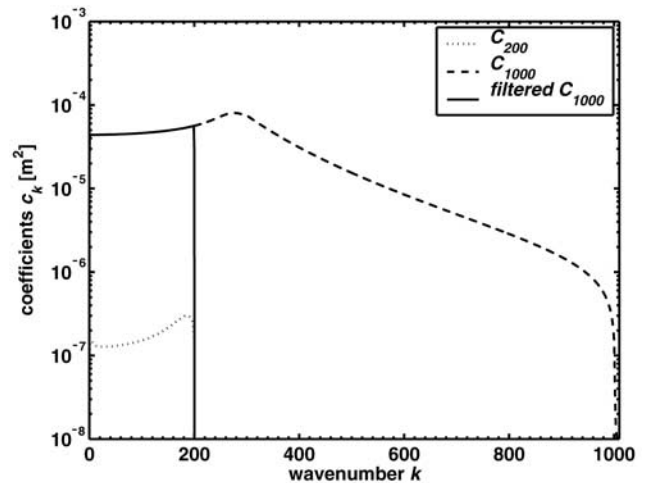

Figure 4. Fourier spectra of geoid height error covariance functions: commission error up to $L = 200$ (C_{200}), commission plus omission error (C_{1000}), and a filtered version of the latter with cut-off $k = 200$.

now describes the shortest wavelength $2\pi R/k$ contained in the covariance function.

3.   A Simple Section Model

[30]   In this section we use a very simple model, based on geostrophy, that mimics the more complex inverse box model of the following section, to demonstrate the problem discussed in section 2. The model consists of one section through an arbitrary ocean of constant depth with one integral conservation equation for volume. This section could close a marginal sea, for example, thus forming a closed "box" with the coastlines. The volume of the water is conserved in the box. We assume no vertical shear in velocity but consider only the vertically constant velocity component, so that the unknowns are the surface velocities v. They can be calculated from sea-surface topography by

$$v = \frac{g}{f} \frac{\partial \zeta}{\partial x}, \qquad (11)$$

where g is the acceleration due to gravity and f is the Coriolis parameter. Spherical harmonic functions are clearly not the proper basis to describe the unknown velocities. We will show the impact of the change of basis by investigation of the posterior errors of the transport through the section.

3.1.   Model Without Sea-Surface Topography Data

[31]   For the hydrographic model without sea-surface topography, we choose a zonal section with 61 stations along $30°S$. The station spacing is constant with $\Delta x_j = 0.5°$ longitude. The depth at each station pair is $D = 4000$ m. The only conservation equation is

$$D \sum_j v_j \Delta x_j = \phi + \delta\phi. \qquad (12)$$

The actual values for the unknown velocities v_j do not matter in this investigation, as the model is linear. We choose them to be zero. We assume that the transport ϕ is zero within $\delta\phi = \pm 10$ Sv (1 Sv = 10^6 m^3/s). Equation (12) can be rewritten in matrix form

$$\mathbf{M}_0\mathbf{x} = \mathbf{y}_0 + \mathbf{n}_0, \qquad (13)$$

where $\mathbf{x}$ is the vector of unknown velocities, $\mathbf{y}_0 = \phi$, and $\mathbf{n}_0 = \delta\phi$. In this sense, the matrix operator $\mathbf{M}_0$ maps the surface velocities onto the total volume transport. The index 0 indicates that this is the zero order information available before adding sea-surface topography data. We estimate a new $\mathbf{x}_0$ by minimizing

$$J = \frac{1}{2}\mathbf{n}_0^T\mathbf{R}_0^{-1}\mathbf{n}_0 + \frac{1}{2}(\mathbf{x}_0 - \mathbf{x}_{00})^T\mathbf{P}_{00}^{-1}(\mathbf{x}_0 - \mathbf{x}_{00}), \qquad (14)$$

with the a priori estimate $\mathbf{x}_{00} = 0$ m/s, the a priori covariance $\mathbf{P}_{00} = \text{diag}(0.01 \text{ m/s})^2$ of this estimate and the error covariance $\mathbf{R}_0 = \delta\phi^2$ of the conservation equation. The error estimates represent typical values for the quantities $\mathbf{P}_{00}$ and $\delta\phi$ [e.g., *Macdonald*, 1998; *Ganachaud and Wunsch*,

2000; *Sloyan and Rintoul*, 2001b]. The solution to this problem is a Gauss-Markov estimate [*Wunsch*, 1996] of the form

$$\mathbf{x}_0 = \mathbf{x}_{00} + \mathbf{K}_0(\mathbf{y}_0 - \mathbf{M}_0\mathbf{x}_{00}), \qquad (15)$$

with the posterior error covariance or uncertainty

$$\mathbf{P}_0 = \mathbf{P}_{00} - \mathbf{K}_0\mathbf{M}_0\mathbf{P}_{00}, \qquad (16)$$

where

$$\mathbf{K}_0 = \mathbf{P}_{00}\mathbf{M}_0^T\left(\mathbf{M}_0\mathbf{P}_{00}\mathbf{M}_0^T + \mathbf{R}_0\right)^{-1}. \qquad (17)$$

Since we have chosen $\mathbf{y}_0 = \mathbf{M}_0\mathbf{x}_{00}$, the new estimate $\mathbf{x}_0$ is the same as the old one ($\mathbf{x}_{00}$), except for a reduced error covariance. Equations (15), (16), and (17) can also be interpreted as the first step of recursively improving the estimate of $\mathbf{x}$: for the nth set of equations we would have

$$\mathbf{x}_n = \mathbf{x}_{n-1} + \mathbf{K}_n\left(\mathbf{y}_n - \mathbf{M}_n\mathbf{x}_{n-1}\right)$$
$$\mathbf{P}_n = \mathbf{P}_{n-1} - \mathbf{K}_n\mathbf{M}_n\mathbf{P}_{n-1}$$

and

$$\mathbf{K}_n = \mathbf{P}_{n-1}\mathbf{M}_n^T\left(\mathbf{M}_n\mathbf{P}_{n-1}\mathbf{M}_n^T + \mathbf{R}_n\right)^{-1}.$$

[32]   When we add more equations recursively, we expect that the error covariance is reduced even further. In particular, when using sea-surface topography data the inclusion of more and more spherical harmonic functions of a geoid model increases the resolution and the accuracy of the resulting sea-surface topography. Although the accuracy of the spherical harmonic coefficients decreases with increasing degree, we expect, from a naive point of view, that more coefficients always mean more information. This gain of information should be reflected in a decrease of the posterior error covariance matrix for the velocities until very high degrees l are reached, for which the errors are so large that on these scales the sea-surface topography data contains no useful information. Especially for an observable such as the horizontally integrated total volume transport ϕ, the short-scale, noisy data should not lead to any improvement. On the other hand, the addition of noisy data should not, again according to naive intuition, degrade the estimate of any observable, in particular not that of a horizontally integrated quantity. However, from the discussion of the sea-surface topography errors in section 2, we anticipate that spherical harmonic functions of high l contribute to the long wavelength components of the estimated velocities.

3.2.   Model With Sea-Surface Topography Data

[33]   The model sea-surface topography at the jth station is calculated from the velocity between the ith station pairs by

$$\zeta_j = \sum_{i=1}^{j} \frac{f_i}{g} v_i \Delta x_i - \zeta_0, \qquad (18)$$

which is the discretized integration of equation (11). The integration constant ζ_0 can be set to zero for our purposes.

The matrix analogue of this equation to equation (13) is

$$M_\zeta x = \zeta^* + n_\zeta. \tag{19}$$

The "measurement" vector ζ^* is obtained by substituting x_0 for x in equation (19). We assume the altimeter measurement to be perfect, so that the error covariance matrix R_ζ is calculated from the geoid error covariance function (5). Since the maximum resolution of the geoid model is generally lower than that of the ocean model, R_ζ does not describe errors on the short scales of the model. In fact, if we sought a new Gauss-Markov estimate of x with equations (19) and a low resolution error covariance of the sea-surface topography, we would implicitly assume that on the short scales the data have an error of zero. We therefore have to modify the operator M in equation (19), so that only the scales described by the geoid error covariance are included in the calculation. In other words, we need to filter the model's sea-surface topography estimate before we can compare it to the sea-surface topography data in equation (19). In order to design a filter, we diagonalize R_ζ. If the section is long enough so that $n/2$ waves of wavelength $2\pi R/L$ fit into it, the eigenvalue spectrum of R_ζ drops sharply to zero after n eigenvalues. Only these n eigenvalues are kept and the equations (19) are expanded into the corresponding eigenfunctions of the error covariance matrix R_ζ:

$$M_L^{(\zeta)} x = y_L + n_L, \tag{20}$$

with $M_L^{(\zeta)} = V_L^T M_\zeta$, $y_L = V_L^T \zeta^*$. The columns of matrix V_L are the eigenvectors corresponding to the kept eigenvalues σ_L^2. $M_L^{(\zeta)} x$ is the vector of coefficients of the expansion of $M_\zeta = V_L M_L^{(\zeta)} x$. Because we use the eigenvectors V_L of the geoid model error covariance matrix, we make sure that only those structures that the sea-surface topography data can describe are compared in equation (20). By construction, these can only be long scales, as the error covariance matrix does not contain high degrees (higher than maximum degree L). Note that our procedure is similar to the truncated SVD solution of *Wunsch* [1978], where only the resolved data structures are kept to construct the flow field.

[34] The error R_L is then a diagonal $n \times n -$ matrix with the eigenvalues $\sigma_{1, \dots, n}^2$ as diagonal elements. The subscript L indicates that the number of eigenvalues and the eigenvectors themselves depend on the maximum degree L used in the geoid model. The analogous recursive Gauss-Markov estimate to equations (15), (16), and (17) is

$$x_L = x_0 + K_L(y_L - M_L x_0) \tag{21}$$

$$P_L = P_0 - K_L M_L P_0 \tag{22}$$

$$K_L = P_0 M_L^T (M_L P_0 M_L^T + R_L)^{-1}. \tag{23}$$

Again, since we have chosen ζ^* so that $y_L - M_L x_0 = 0$, only the posterior error estimate is affected by the new equations. These new equations either decrease the posterior error estimates or leave them unchanged.
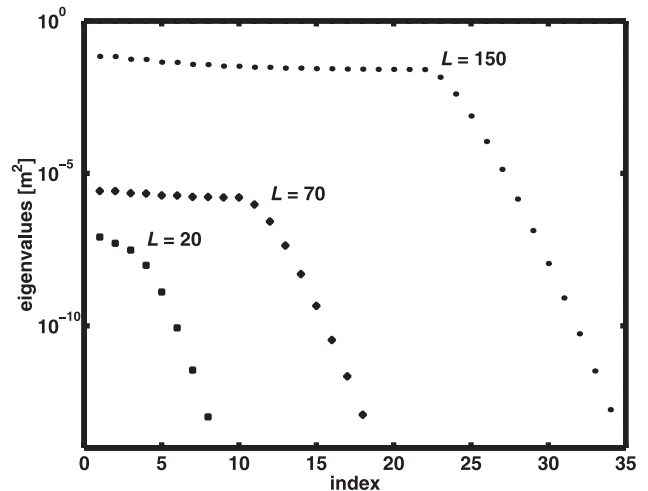

Figure 5. Eigenvalue spectrum of the geoid error covariance matrix for the three cases $L = 20$, $L = 70$, and $L = 150$.

[35] For the following experiments we use the expected error spectrum of the GRACE mission, since the geoid model resulting from this mission will have very small errors for low degrees l (Figure 1). The error spectrum increases almost exponentially with degree. It is therefore ideal for demonstrating the effect of large errors of high degrees on long scales.

3.3. Results and Discussion

[36] The posterior error of the total volume transport $\sqrt{M_0 P_n M_0^T}$ for the hydrographic model without sea-surface topography data is 8.4 Sv. So the assumption of an error of 1 cm/s for the barotropic velocities reduces the prior error estimate of the volume transport of 10 Sv by 16%.

[37] We decided to use three different cutoff degrees for the model with sea-surface topography: $L = 20$, which is representative of the very long wave range, $L = 70$, the range for which GRACE is expected to improve the present geoid models, and $L = 150$, where the error estimate intersects Kaula curve. The wavelengths associated with these degrees are 2000, 570, and 270 km, respectively. The corresponding eigenvalue spectra drop after 3, 11, and 22 eigenvalues (Figure 5).

[38] Note that in general the size of the eigenvalues increases with L. This can be explained as follows: The square root of eigenvalues describes the error of the data coefficients y_L. The error increases with L because more structures of the data are kept in the calculation. For small L the errors of these new structures contribute to the omission error.

[39] For $L = 20$ the posterior transport error is reduced to 4.0 Sv. Using a geoid model to degree $L = 70$ approximately halves this error again to a value of 1.9 Sv. Here the result meets our naive expectation that additional resolution of the geoid model improves the estimate of the total transport. However, increasing L to 150 increases the posterior error again to 3.9 Sv. In this section, as opposed to section 2, the basis functions are not sines and cosines but the eigenfunctions of the geoid error covariance matrix. In this sense we have used the presuppositions of the geoid model as much as possible.
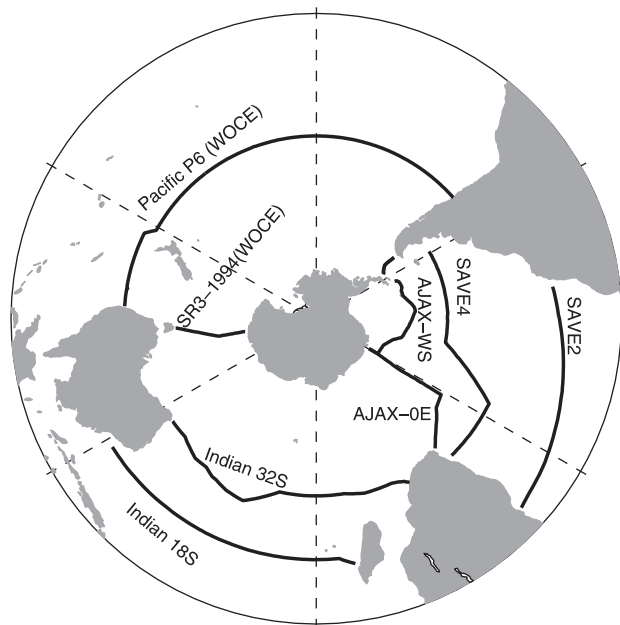
Figure 6. Position of hydrographic sections, box regions, and constraints used in the inverse model.

[40] Although a geoid model to degree $L = 150$ contains more information than one to degree $L = 70$, its impact on the posterior volume transport error of this section model is smaller than for the coarse geoid model. The large-scale volume transport is already well determined by low degrees of the spherical harmonic functions. The precision of these harmonics is diluted by the higher degree functions, whose short scales cannot decrease the transport errors as much as their "leakage" into long waves degrades the quality of the low degree functions. This "leakage" becomes apparent because the spectrum of the geoid model error spans several orders of magnitude. The contributions of high degree spherical harmonics to long wavelengths, which decrease rapidly for decreasing wave number k, are amplified by the large error coefficients (see equation (8)).

4. Box Inverse Model of the Southern Ocean

[41] For the purpose of this study we use the Southern Ocean inverse model of *Sloyan and Rintoul* [2000, 2001a, 2001b], which is based on *Wunsch* [1978]. The inverse box model defines a system of conservation equations, derived from hydrographic sections, that can be written in the same matrix form as equation (13). $\mathbf{M}_0$ is a matrix whose elements are the area × property concentration (for the properties mass, temperature, salt) at each station pair in each layer, and for each layer interface; $\mathbf{y}_0$ is the property divergence in each layer due to relative (baroclinic) and Ekman fluxes and $\mathbf{x}$ is the vector of unknown reference (barotropic) velocities, diapycnal property transfer rates, and corrections to air-sea climatologies.

[42] The model noise is $\mathbf{n}_0$. Again, the index 0 indicates that this is the information available before the addition of sea-surface topography data. The Gauss-Markov estimate of this system is completely analogous to equations (15), (16), and (17) with $\mathbf{x}_{00} = 0$, since we will choose the

reference velocities to be at an estimated level of no motion with prior errors of $(0.01 \text{ m/s})^2$ for midbasin stations and $(0.06 \text{ m/s})^2$ at western boundaries [*Macdonald*, 1998; *Ganachaud and Wunsch*, 2000; *Sloyan and Rintoul*, 2001b].

[43] The inclusion of sea-surface topography data is also absolutely analogous to the simplified model of section 3.3. We choose $\zeta^* = \mathbf{M}_\zeta \mathbf{x}_0$, so that again $\mathbf{y}_L - \mathbf{M}_L \mathbf{x}_0 = 0$. The prior errors of ζ^* are estimated for each section separately as described in section 3.2. This way the total covariance matrix for sea-surface topography is block-diagonal; that is, small correlations which exist between different sections are neglected in our calculations.

4.1. Hydrographic Data, Model Domain and A Priori Constraints

[44] The inverse model of *Sloyan and Rintoul* [2000, 2001a, 2001b] used nine hydrographic sections to define six "boxes" in the Southern Hemisphere oceans (Figure 6). Twenty-three neutral density [*Jackett and McDougall*, 1997] layers were chosen to span the water masses in the model domain, and the following a priori assumptions were used to constrain the general circulation produced by the model (see also Figure 6): (1) -0.8 ± 2 net southward transport at SAVE2 [*Coachman and Aagaard*, 1988; *Wijffels et al.*, 1992]; (2) 4 ± 2 northward bottom water transport in Brazil basin [*Hogg et al.*, 1982; *Speer and Zenk*, 1993]; (3) 0 ± 2 net transport into the Weddell Sea and 16 ± 5 Wm^{-2} heat loss over the Weddell Sea [*Gordon and Huber*, 1990; *Fahrbach et al.*, 1994]; (4) 60 ± 5 northward Malvinas Current [*Peterson and Stramma*, 1991; *Peterson*, 1992]; (5) 6 ± 2 northward transport of AABW across Argentine basin [*Whitworth et al.*, 1991]; (6) 11 ± 5 northward transport of LCDW/AABW coincident with WOCE PCM-9 (P32) [*Whitworth et al.*, 1999]; and (7) O(500 kmols^{-1}) Silica conservation all regions [*Trèguer et al.*, 1995].

4.2. Hydrographic Estimate of the Mean Circulation

[45] A description of the net meridional and zonal fluxes (Table 1) and a general description of the mean circulation is given below. This is provided to familiarize the reader with the gross circulation features of the model. For a more thorough description the reader is referred to *Sloyan and Rintoul* [2000, 2001a, 2001b].

[46] Across the Atlantic, there is a small net southward volume transport which corresponds to the leakage of Pacific water through Bering Strait into the North Atlantic

Table 1. Total Section Volume and Temperature Transports[a]

Section	Mass, Sv	Heat, PW
SAVE2	-0.82 ± 0.39	0.49 ± 0.06
SAVE4	-0.31 ± 1.60	0.37 ± 0.05
DP	137.5 ± 6.6	1.44 ± 0.05
SA	138.5 ± 7.0	1.12 ± 0.09
WS	0.01 ± 0.20	-0.05 ± 0.004
I18	-7.40 ± 4.02	-1.28 ± 0.19
I32	-8.14 ± 3.71	-0.79 ± 0.14
SR3	146.7 ± 7.3	1.72 ± 0.09
P32	7.31 ± 3.20	0.36 ± 0.13

[a] 1 Sv = 10^6 m^3/s, 1 PW = 10^{15} J/s, positive values refer to northward or eastward transports, temperature transports are relative to 0°C.
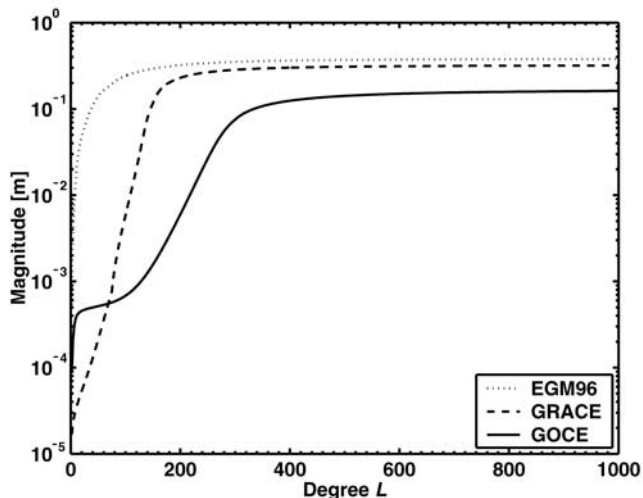
Figure 7. Cumulative geoid error as a function of maximum degree L for EGM96, GRACE, and GOCE. The curves are extended to $L = 1000$ with Kaula's law.

Ocean (Table 1). The mass flux between SAVE2 and SAVE4 decreases slightly because of the dominance of evaporation over precipitation in the subtropical South Atlantic. The southward transport of 18 ± 4 Sv of North Atlantic Deep Water (NADW) agrees with previous estimates [*Dickson and Brown*, 1994; *Rintoul*, 1991; *McCartney*, 1993]. The NADW overturning cell is close by northward transport of thermocline and intermediate water, which results in a northward temperature transport across the Atlantic of 0.37 ± 0.05 PW at SAVE4 and 0.49 ± 0.06 PW at SAVE2 (1 PW = 10^{15} J/s). These values agree with those of *Macdonald* [1998] of 0.49 ± 0.25 PW and those of *Saunders and King* [1995] of 0.5 ± 0.1 PW.

[47] In the Indian Ocean there is a southward volume transport at $18°$S and $32°$S of 7 ± 4 Sv and 8 ± 4 Sv, respectively (Table 1). The increased volume transport between I18 and I32 is not significant and within the a priori model noise of $O(1-2)$. The southward flow corresponds to the size of the Indonesian Throughflow and is within reasonable agreement of recent estimates [*Cresswell et al.*, 1993; *Meyers et al.*, 1995].

[48] Across $32°$S in the Pacific Ocean, there is a net northward volume transport of 7 ± 3 Sv. This results from a net northward flux of thermocline layers. The temperature transport across $32°$S of 0.36 ± 0.13 PW is larger than the heat flux estimates by *Macdonald* [1998] of -0.04 ± 0.32 PW at $28°$S and 0.26 ± 0.28 PW at $43°$S.

[49] In the Southern Ocean the Antarctic Circumpolar Current (ACC) dominates the three choke point sections with an eastward volume transport of 137.5 ± 7 Sv at Drake Passage, 138.5 ± 7 Sv south of Africa, and 146.7 ± 7 Sv south of Australia (Table 1). The property divergences between the choke point sections result from imports or exports across the three southern subtropical sections and changes to the water layer composition between the choke point sections. The largest divergences occur between south of Africa and south of Australia. The increases in eastward property transports south of Australia result from the inclusion of Indonesian Throughflow water

in the Indian sector and their eastward transport with the ACC.

4.3. Experiments With Sea-Surface Height Data

[50] We study the impact of different a priori assumptions about the geoid model error, thus its covariance matrix. Three covariances are available: EGM96 [*Lemoine et al.*, 1997] to degree and order $L = 70$ and one estimate each of the geoid covariances for the future GRACE and GOCE missions [*Balmino et al.*, 1998]. The latter two are available to degree and order $L = 150$ and $L = 300$, respectively, where they attain maximum resolution. However, we choose lower resolutions (half wavelength), namely 286 km ($L = 70$) for GRACE and 100 km ($L = 200$) for GOCE. These choices correspond to the respective scales, which the geoid missions are designed to resolve. In fact, the curves of the cumulative geoid error as a function of maximum degree L of GRACE and GOCE intersect at $L \approx 70$ (Figure 7), so that GRACE is expected to perform better than GOCE only for $l < 70$.

[51] Although the EGM96 geoid's maximum degree is 360, its error covariance is only complete to degree and order 70 and the remaining part is a diagonal variance. This variance is used for estimating the error contribution from $l = 71$ to 360.

[52] We show two suites of experiments. The first set consists of the model which includes the sea-surface topography data weighted by the geoid error up to the maximum degree L corresponding to the resolution of EGM96 ($L = 70$), GRACE ($L = 70$), and GOCE ($L = 200$). This set of experiments has been previously discussed by *Schröter et al.* [2002], their Experiment B. The "design" of the geoid error used in these experiments is basically the same as in other studies [e.g., *Ganachaud et al.*, 1997; *LeGrand*, 2001] and appears to be generally accepted. In the current study we label this set of experiments NOM (no omission error).

[53] In a second set of experiments we take the extreme point of view, that all of the geoid omission error has a contribution to the long wavelengths. For each geoid model, we include the omission error to degree $L = 1000$ and then remove the short scales by applying a low-pass filter as described in section 2.2. This set of experiments is labeled FOM (full omission error).

[54] For all experiments the altimeter measurement errors C_h are assumed to be 4 cm [*Tapley et al.*, 1994] and white on the model grid scale. Their diagonal error covariances have to be low-pass filtered to remove uncorrelated errors on scales shorter than the geoid resolution. This is done in analogy to filtering the geoid error covariance in section 2.2 with a Butterworth filter. For a more detailed description see *Schröter et al.* [2002]. In all cases, sea-surface topography error covariances are calculated separately for each section. This way small error correlations between sections that do exist are neglected.

[55] The sea-surface topography "data" are calculated from the model solution with hydrographic data only described in the previous section, so that as in section 3, $\mathbf{y}_L = \mathbf{M}_L \mathbf{x}_0$. The new solutions with sea-surface topography data will only be different from the solution without sea-surface data in their posterior error estimates.

[56] Figure 8 shows all six sea-surface topography error covariance matrices R_ς, for the sample hydrographic section
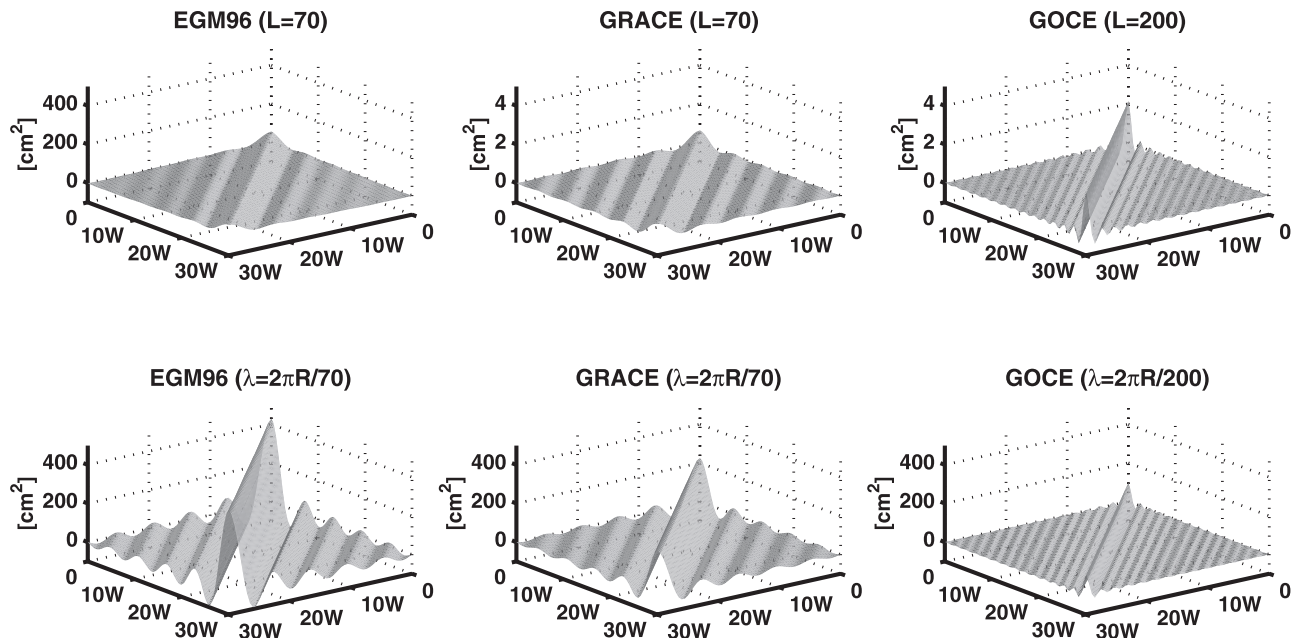
Figure 8. SSH error covariance matrices $\mathbf{R}_\zeta$ (top) without omission error (note the different scale for GRACE and GOCE) and (bottom) with omission error after filtering out all small scales according to the maximum degree and order used for EGM96, GRACE, and GOCE, for the zonal sample section of section 3.

of section 3. Comparing the covariance matrices from left to right, the different scales included in estimating these errors become apparent by the "sharper" main diagonal of the error covariances of the GOCE geoid model error. In the case when the geoid omission error is not included (top), the GOCE geoid model describes far more wavelengths than the other geoid models and its error variance is larger than the error variance of the GRACE geoid model. This situation is reversed when the geoid omission error is taken into account (bottom). Comparing Figure 8 (top) with Figure 8 (bottom), all variances have increased (note the change in scale between the top and bottom panels). In the case of GRACE and GOCE, the increase is two orders of magnitude. Also the GRACE omission error is much larger than that of GOCE. Therefore including the effects of the omission error on the long wavelengths increases the GRACE variance by more than the GOCE variance. Thus not only do the scales become smaller from left to right in Figure 8 (bottom) but also the size of the variances, that is, the errors decrease. Here including the omission error to degree $L = 1000$ makes the performance of GRACE worse than that of GOCE; it does so even at the wavelength $\lambda = 2\pi R/70$ and in spite of the small per-degree-errors of GRACE for the low degrees. Again, we point out that the "leakage" of omission into commission error is due to a change of basis functions. Although GRACE and GOCE have small errors at low degrees, the geoid error dominates the total error even at large scales ($> \lambda = 2\pi R/L$) when the omission error is included.

[57] In the discussion of the experiments it is useful to remember that a priori constraints on the property flux across some hydrographic sections, based on hydrographic information, are imposed. For example, conservation of mass dictates zero mass flux across the Weddell Sea (WS)

and a small net southward volume transport across the transatlantic section at 12°S (SAVE2) with small prior errors, whereas the transport through Drake Passage or south of Australia (SR3) cannot be fixed to precise values a priori. Therefore the posterior errors in the solution from hydrography alone are large for the latter type of sections and an order of magnitude smaller for the former. For those sections with very small prior errors, noisy SSH data cannot add much new information. Only across hydrographic sections with large prior errors would we expect a considerable reduction in the posterior errors due to inclusion of SSH data.

[58] Figure 9 summarizes the experiments with sea-surface topography data in terms of the percent (%) error reduction relative to the base experiment without sea-surface topography for the volume and temperature transport. No values for the Weddell Sea section are shown because the sea-surface topography data has no visible impact due to small prior errors on the transports.

[59] *Schröter et al.* [2002] discuss the experiments which exclude the geoid omission error (NOM, left-hand side of Figure 9). They conclude that improvements of transport estimates with sea-surface topography data relative to EGM96 is smaller than 10% (NOM, left-hand side of Figure 9, first columns). Furthermore, they point out that when using real sea-surface topography data instead of values taken from a previous model run, the inverse model yielded unrealistic results (not shown). With the expected geoid error estimates from GRACE and GOCE, there is an average reduction of posterior error estimates of 16% for sections with a priori constraints for transport estimates (i.e., SAVE2, SAVE4) and 54% for sections without such prior assumptions (i.e., SR3, DP, and SA). The additional effect of a higher GOCE resolution is small compared to the
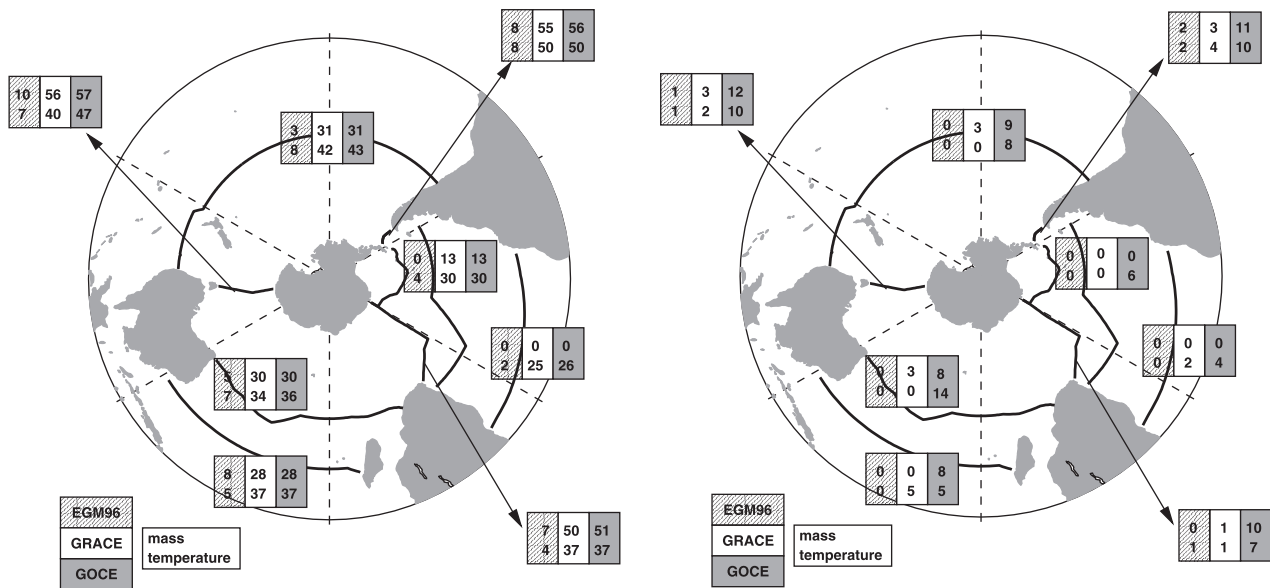
Figure 9. Error reduction relative to hydrography alone solution (left) without omission error (NOM) and (right) with omission error (FOM). The upper numbers are the error reductions of mass transports (in %), the lower numbers those of temperature transports.

results with the GRACE geoid model. To *Schröter et al.* [2002], this came as a surprise as the latter is only accurate on long scales.

[60] The right-hand side of Figure 9 shows the error reduction (in percent) for the FOM-experiments relative to the base experiment without sea-surface topography data. Compared to the NOM experiments, the FOM posterior error improvements over the base experiment are greatly reduced when the geoid omission error is included in the error estimates of the sea-surface topography data. This is expected because the prior sea-surface topography errors are much larger for the FOM experiments. The greatest improvement possible with GOCE is now of the order of 10%, ~5 times smaller than in the case without geoid omission error. EGM96 shows only a minimal improvement, and even the long scales accurate GRACE geoid model shows little posterior transport error reduction.

[61] The error reduction has a different dependence on the resolution of the sea-surface topography for each geoid model. The GRACE geoid model, due to its low resolution, has a very large omission error. Therefore the improvements obtained with this model are not significantly greater than that achieved with the much less accurate EGM96 geoid model. Because of the high resolution of the GOCE geoid model, i.e., smaller errors at small scales, the omission error of this model is smaller than that of the EGM96 and GRACE. Therefore, in the FOM experiments GOCE provides larger improvement in the posterior transport errors than those of the low resolution EGM96 and GRACE geoid models, although the FOM GOCE geoid model results in a smaller improvement when compared to NOM GOCE. With the FOM GOCE geoid model the best transport estimates can be obtained with an improved accuracy of between 10–14% over the baseline experiment without sea-surface topography.

[62] In general, when the omission error to degree $L = 1000$ is included in the error estimates of the sea-surface

topography data, the possible posterior error reduction for transport estimates is disappointing. However, we do not claim that our approach is correct. We juxtaposed the two different ways of estimating the geoid errors because we wanted to demonstrate the effect that the omission error might have on the long, supposedly well-known, scales. How (or if) to properly account for the geoid omission error, must be the topic of further research.

5. Discussion and Conclusion

[63] We have shown that defining a scale for spherical harmonics in the context of oceanographic applications has some difficulties; Legendre polynomials of high degree contribute to low Fourier wave numbers as a consequence of changing the orthonormal basis. Usually this contribution is small. Omitting high degrees appears to be appropriate when dealing with geoid models for which the coefficients of the spherical harmonics decrease with increasing degree l according to Kaula's rule of thumb ($\propto l^{-2}$). However, the spectral coefficients of the geoid model errors are very small for low degrees and increase rapidly by several orders of magnitude for high degrees. This is especially true for the errors of the future geoid models GRACE and GOCE. Neglecting the geoid omission error (which consists of the high degrees) might lead to a serious underestimation of the total geoid error on long scales.

[64] This problem was demonstrated with the use of a simple (idealized) barotropic box model and a realistic box inverse model of the Southern Ocean. In both cases, the basis functions of the model domains were not the Fourier functions but the eigenfunctions of the geoid error covariance matrix evaluated along the section. The original Gauss-Markov estimate of each model was improved by including sea-surface topography data. However, in the idealized model, continual addition of information (in the

form of more coefficients of higher degree) eventually led to an increase of the a posteriori estimated errors of the total volume transport through the section. Therefore, contrary to naive intuition, supplying more data led to a smaller gain of information by the model.

[65] In the Southern Ocean box inverse model, the omission error of the EGM96 and the future gravity missions GRACE and GOCE, calculated to degree 1000, was included in the geoid error estimates. The improvement in the error estimate by the inclusion of sea-surface topography data over that of a hydrographic only model was compared and contrasted with earlier results of *Schröter et al.* [2002]. This earlier study uses the same Southern Ocean box inverse model but completely neglected the omission error, which appears to be common practice. In both cases, three different geoid error estimates are used: EGM96, GRACE, and GOCE. The prior error estimates for the sea-surface topography data are much larger when the geoid omission error is included. It is therefore not surprising that in this study the possible improvements of transport estimates are much smaller than those found by *Schröter et al.* [2002]. We also found that the improvements from the on-low-degrees-highly-accurate GRACE geoid model and the imprecise EGM96 geoid model are almost negligible when the omission error of both geoid models is taken into account. GRACE has a large omission error because its low resolution contributes to errors on the long scales. If one includes the geoid omission error to degree 1000, only the high resolution GOCE geoid model, due to its comparatively small omission error, will improve oceanic transport estimates from box inverse models. We have chosen to include the omission error to degree 1000 to emphasize the full effect the omission error has on the long scales of the ocean model. A smaller omission error (e.g., to degree 300) would not change our conclusion, namely that the geoid omission error needs to be accounted for. However it would have made the effects of the omission error less obvious.

[66] Our results show that the impact of the geoid omission error on estimates of the ocean circulation is not negligible. It is now necessary to find ways to deal with this error. Clearly, taking into account the entire geoid error to degree 1000 overestimates the actual error and we have expressed our concerns about the validity of this approach earlier in the paper. Since the dynamic sea-surface topography is the difference between altimetric measurement and geoid undulation, the omission error of the altimetry will cancel out some of the omission error of the geoid model. This is not in conflict with equation (1) because omission errors are actually unmodeled signals. Also, the model estimate of the sea-surface topography, owing to the finite resolution of the model grid, has an omission error as well which needs to be described in the cost function, thus in the error estimates. However, this cancellation of omission error will not be complete because the spectral characteristics of the three types of errors, inverse model, geoid, and altimetry, are different. Furthermore, the omission error of altimetry is most likely anisotropic as the resolution of the altimetric measurement is very high along track, where the omission error is probably negligible, and considerably lower in the across track direction. For the TOPEX/Poseidon satellite the track separation is on the order of 100 km.

[67] A possible remedy might be a filter that has similar spectral properties in all domains of interest. *Jekeli* [1981] proposed a nearly Gaussian filter to improve the Earth's gravity field. This filter has been used by *Wahr et al.* [1998] to investigate whether it will be possible to detect hydrological and oceanic effects on the time variability of the Earth's gravity field. Since this filter is nearly Gaussian, its spectral representation is also nearly Gaussian for spherical harmonic coefficients. As an approximation, its spectral response in Fourier space can be taken as that of a truly Gaussian cap, making the problem of "leakage" of high degree spherical harmonics into low Fourier wave number functions smaller. However, one major drawback of a Gaussian filter is its high attenuation in the pass band. The omission error of geoid models needs to be taken into account when estimating the error of absolute sea-surface topography data. How this should be done is subject to further investigations.

Notation

C error covariance function
$\mathbf{P}$ error covariance matrix of independent variables
$\mathbf{R}$ model error covariance matrix
$\mathbf{M}$ model operator
ζ (absolute) sea-surface topography
h sea-surface height relative to reference ellipsoid
N geoid height, geoid undulation
P_l Legendre polynomial
P_{lm} associated Legendre function
Y_{lm} spherical harmonic function
AABW   Antarctic Bottom Water
NADW   North Atlantic Deep Water
IDW   Indian Deep Water
PDW   Pacific Deep Water
LCDW   Lower Circumpolar Deep Water
ACC   Antarctic Circumpolar Current
WOCE   World Ocean Circulation Experiment
EGM96   Earth Gravitational Model 1996
GRACE   Gravity Recovery and Climate Experiment
GOCE   Gravity field and steady state Ocean Circulation Explorer

References

Balmino, G., F. Perosanz, R. Rummel, N. Sneeuw, H. Sünkel, and P. Woodworth, European views on dedicated gravity field missions: GRACE and GOCE, An Earth Sciences Division Consultation Document, ESD-MAG-REP-CON-001, Eur. Space Agency, Paris, 1998.

Battrick, B. (Ed.), *Gravity Field and Steady-State Ocean Circulation Explorer*, ESA SP-1233 (1) — The Four Candidate Earth Explorer Core Missions, Eur. Space Agency, Paris, 1999.

Bell, M. J., R. M. Forbes, and A. Hines, Assessment of the FOAM global data assimilation system for real-time ocean forecasting, *J. Mar. Syst.*, *25*, 1–22, 2000.

Coachman, L., and K. Aagaard, Transport through Bering Strait: Annual and interannual variability, *J. Geophys. Res.*, *93*, 15,535–15,539, 1988.

Cresswell, G. R., A. Frische, J. Peterson, and D. Quadfasel, Circulation in the Timor Sea, *J. Geophys. Res.*, *98*, 14,379–14,389, 1993.

Dickson, R. R., and J. Brown, The production of North Atlantic Deep

Water: Sources, rates and pathways, *J. Geophys. Res.*, *99*, 12,319–12,341, 1994.

Egbert, G., Tidal data inversion: Interpolation and inference, *Prog. Oceanogr.*, *40*, 53–58, 1997.

Fahrbach, E., G. Rohardt, M. Schröder, and V. Strass, Transport and structure of the Weddell Gyre, *Ann. Geophys.*, *12*, 840–855, 1994.

Fu, L.-L., Mass, Heat and Freshwater fluxes in the South Indian Ocean, *J. Phys. Oceanogr.*, *16*, 1683–1693, 1986.

Fukumori, I., Assimilation of TOPEX sea level measurements with a reduced-gravity, shallow water model of the tropical Pacific Ocean, *J. Geophys. Res.*, *100*, 25,027–25,039, 1995.

Ganachaud, A., and C. Wunsch, Improved estimates of global ocean circulation, heat transport and mixing from hydrographic data, *Nature*, *408*, 453–457, 2000.

Ganachaud, A., C. Wunsch, M.-C. Kim, and B. Tapley, Combination of TOPEX/POSEIDON data with a hydrographic inversion for determination of the oceanic general circulation and its relation to geoid accuracy, *Geophys. J. Int.*, *128*, 708–722, 1997.

Gordon, A. L., and B. A. Huber, Southern Ocean winter Mixed Layer, *J. Geophys. Res.*, *95*, 11,655–11,672, 1990.

Hernandez, F., and P. Schaeffer, Altimetric mean sea surfaces and gravity anomaly maps inter-comparisons, *AVISO techn. rep. AVI-NT-011-5242-CLS*, CLS, Toulouse, France, 2000.

Hogg, N. G., P. Biscaye, W. Gardner, and W. J. Schmitz Jr., On the transport and modification of Antarctic Bottom Water in the Vema Channel, *J. Mar. Res.*, *40*, 231–263, 1982.

Jackett, D., and T. J. McDougall, A neutral density variable for the worlds oceans, *J. Phys. Oceanogr.*, *27*, 237–263, 1997.

Jekeli, C., Alternative methods to smooth the Earth's gravity field, *Tech. Rep. 327*, Dep. of Geodetic Sci. and Surveying, Ohio State Univ., Columbus, 1981.

Kaula, W. M., *Theory of Satellite Geodesy*, Blaisdell Publ. Company, Waltham, Mass., 1966.

Kulhánek, O., *Introduction to Digital Filtering in Geophysics*, Elsevier Sci., New York, 1976.

LeGrand, P., Impact of the Gravity Field and Steady-State Ocean Circulation Explorer (GOCE) mission on ocean circulation estimates: Volume fluxes in the climatological inverse model of the Atlantic, *J. Geophys. Res.*, *106*, 19,597–19,610, 2001.

Lemoine, F. G., et al., The development of the NASA GSFC and NIMA joint geopotential model, in *Gravity, geoid and marine geodesy*, edited by J. Segawa, H. Fujimoto, and S. Okubo, vol. 117, pp. 461–469, Int. Assoc. of Geodesy Symp., Springer-Verlag, New York, 1997.

Le Provost, C., F. Lyard, J. Molines, M. Genco, and F. Rabilloud, A hydrodynamic ocean tide model improved by assimilating a satellite altimeter-derived data set, *J. Geophys. Res.*, *103*, 5513–5529, 1998.

Macdonald, A. M., The global ocean circulation: A hydrographic estimate and regional analysis, *Prog. Oceanogr.*, *41*, 281–382, 1998.

Malanotte-Rizzoli, P., (Ed.), *Modern Approaches to Data Assimilation in Ocean Modelling*, 455 pp., Elsevier Sci., New York, 1996.

McCartney, M. S., Crossing of the equator by the Deep Western Boundary Current in the western Atlantic Ocean, *J. Phys. Oceanogr.*, *23*, 1953–1974, 1993.

Meyers, G., R. J. Bailey, and A. P. Worby, Geostrophic transport of Indonesian throughflow, *Deep-Sea Res.*, *42*, 1163–1174, 1995.

Pedlosky, J., *Geophysical Fluid Dynamics*, 710 pp., Springer-Verlag, New York, 1987.

Peterson, R., The boundary currents in the western Argentine basin, *Deep Sea Res.*, *39*, 623–644, 1992.

Peterson, R., and L. Stramma, Upper-level circulation in the South Atlantic Ocean, *Prog. Oceanogr.*, *26*, 1–73, 1991.

Rapp, R., Geopotential coefficient behaviour to high degree and geoid information by wavelength, *Tech. Rep. 180*, Dep. of Geodetic Sci., Ohio State Univ., Columbus, 1972.

Rintoul, S. R., South Atlantic interbasin exchange, *J. Geophys. Res.*, *96*, 2592–2675, 1991.

Roemmich, D., and T. McCallister, Large scale circulation of the North Pacific Ocean, *Prog. Oceanogr.*, *22*, 171–204, 1989.

Saunders, P. M., and B. R. King, Oceanic Fluxes on the WOCE A11 Section, *J. Phys. Oceanogr.*, *25*, 1942–1957, 1995.

Schröter, J., M. Losch, and B. M. Sloyan, Impact of the Gravity Field and Steady-State Ocean Circulation Explorer (GOCE) mission on ocean circulation estimates, 2, Volume and heat transports across hydrographic sections of unequally spaced stations, *J. Geophys. Res.*, *107*(C2), 10.1029/2000JC000647, 2002.

Sloyan, B. M., and S. R. Rintoul, Estimates of area-averaged diapycnal fluxes from basin-scale budgets, *J. Phys. Oceanogr.*, 2320–2341, 2000.

Sloyan, B. M., and S. R. Rintoul, Circulation, renewal and modification of Antarctic mode and intermediate water, *J. Phys. Oceanogr.*, *31*, 1005–1030, 2001a.

Sloyan, B. M., and S. R. Rintoul, The Southern Ocean limb of the global deep overturning circulation, *J. Phys. Oceanogr.*, *31*, 143–173, 2001b.

Sneeuw, N., and R. Bun, Global spherical harmonic computation by two-dimensional fourier methods, *J. Geod.*, *70*, 224–232, 1996.

Speer, K. G., and W. Zenk, The flow of Antarctic Bottom Water into the Brazil Basin, *J. Phys. Oceanogr.*, *23*, 2667–2682, 1993.

Stammer, D., C. Wunsch, R. Giering, Q. K. Zhang, and J. Marotzke, The global ocean circulation estimated from TOPEX/POSEIDON altimetry and a general circulation model, *Rep. 49*, Cent. of Global Change Sci., Mass. Inst. of Technol., Cambridge, 1997.

Tapley, B. D., The gravity recovery and climate experiment (GRACE), *Eos Trans. AGU*, *78*(46), Fall Meet. Suppl., F163, 1997.

Tapley, B. D., et al., Precision orbit determination for TOPEX/POSEIDON, *J. Geophys. Res.*, *99*, 24,383–24,683, 1994.

Trèguer, P., D. M. Nelson, A. J. Van Bennekorn, D. J. DeMaster, A. Leynaert, and B. Quèguiner, The Silica balance in the world ocean: A reestimate, *Science*, *268*, 375–379, 1995.

Wahr, J., M. Molenaar, and F. Bryan, Time variability of the Earth's gravity field: Hydrological and oceanic effects and their possible detection using GRACE, *J. Geophys. Res.*, *103*, 30,205–30,299, 1998.

Wenzel, M., J. Schröter, and D. Olbers, The annual cycle of the global ocean circulation as determined by 4D VAR data assimilation, *Prog. Oceanogr.*, *48*, 73–119, 2001.

Whitworth, T., III., W. D. Nowlin Jr., R. D. Pillsbury, and R. F. Weiss, Observations of the Antarctic Circumpolar Current and deep boundary current in the Southwest Atlantic, *J. Geophys. Res.*, *96*, 15,105–15,118, 1991.

Whitworth, T., III, B. A. Warren, W. D. Nowlin Jr., R. D. Pillsbury, and M. I. Moore, On the deep western-boundary current in the Southwest Pacific Basin, *Prog. Oceanogr.*, *43*, 1–54, 1999.

Wijffels, S. E., R. W. Schmitt, H. L. Bryden, and A. Stigebrandt, Transport of freshwater by the oceans, *J. Phys. Oceanogr.*, *22*, 155–162, 1992.

Wunsch, C., The North Atlantic general circulation west of 50° determined by inverse methods, *Rev. Geophys.*, *16*, 583–620, 1978.

Wunsch, C., *The Ocean Circulation Inverse Problem*, Cambridge Univ. Press, New York, 1996.

Wunsch, C., and E. M. Gaposchkin, On using satellite altimetry to determine the gerneral circulation of the oceans with application to geoid improvement, *Rev. Geophys.*, *18*, 725–745, 1980.

Wunsch, C., and D. Stammer, Satellite altimetry, the marine geoid, and the oceanic general circulation, *Ann. Rev. Earth Planet. Sci.*, *26*, 219–253, 1998.

————————

Martin Losch, Department of Earth, Atmospheric, and Planetary Sciences, Massachusetts Institute of Technology, 77 Massachusetts Avenue, Bldg. 54-1523, Cambridge, MA 02139, USA.

Jens Schröter, Alfred-Wegener-Institute for Polar- and Marine Research, Postfach 12 0161, 27515 Bremerhaven, Germany.

Bernadette Sloyan, Department of Physical Oceanography, MS 21, Woods Hole Oceanographic Institution, Woods Hole, MA 02543, USA.

Nico Sneeuw, Institut für Astronomische und Physikalische Geodäsie, Arcisstraße 21, 80290 München, Germany.